CORROSION SCIENCE AND TECHNOLOGY, Vol.25, No.1(2026), pp.1~15 pISSN 1598-6462 / eISSN 2288-6524
[Research Paper] DOI: https://doi.org/10.14773/cst.2026.25.1.1

Effect of Alloy Composition on Pore-widening Induced Structural Evolution and Wettability of Anodic Aluminum Oxide

Jisoo Kim[1,††] and Chanyoung Jeong[1,2,†,††]

[1]*Department of Advanced Materials Engineering, Dong-eui University, Busan 47340, Republic of Korea*
[2]*The Research Institute of Advanced Functional Surface Engineering, Dong-eui University, Busan 47340, Republic of Korea*
(Received January 29, 2026; Revised February 11, 2026; Accepted February 12, 2026)

Anodic aluminum oxide (AAO) is commonly utilized in functional surface engineering, yet the influence of alloy composition on AAO growth behavior, pore-widening (PW) characteristics, and structural stability remains poorly understood. This study investigates AAO films formed on Al 1050, Al 3003, Al 5052, and Al 6061 through anodization for 1 hour under identical conditions, followed by PW in phosphoric acid for varying durations. Despite the same anodizing conditions, significant differences were noted in pore diameter, oxide-film thickness, and AAO growth rates based on alloy composition. Al 5052 demonstrated the highest growth and PW rates, while Al 3003 exhibited the lowest. During the PW process, all alloys initially experienced increased porosity and enhanced wettability; however, extended PW led to distinct collapse behaviors of the oxide film that were dependent on the alloy. These behaviors ranged from gradual structural transformation to rapid oxide removal. Notably, wettability enhancement occurred only while a stable porous structure was intact; once the oxide film collapsed or was removed, wettability reverted. These findings indicate that the PW rate and structural stability are governed by different mechanisms, highlighting the critical role of alloy composition in influencing AAO growth, collapse behavior, and wettability.

Keywords: *Aluminum Alloy, Anodic Aluminum Oxide, Pore-Widening, Structural Stability, Wettability*

1. Introduction

Anodizing is a representative surface treatment technique that enables the formation of various functional surfaces by artificially generating an oxide film on a metal surface, leading to improved corrosion resistance, enhanced durability, and controlled surface wettability [1-3]. In particular, anodic aluminum oxide (AAO) possesses a porous oxide-film structure that allows precise control over pore size and oxide-film thickness, and therefore plays an important role in a wide range of industrial and research fields, including catalyst supports, nanostructure templates, and pretreatment layers for functional coatings [4-6].

To date, studies on AAO have mainly focused on the effects of process parameters such as electrolyte type, applied voltage, temperature, and anodizing time on pore structure and oxide-film growth behavior [7-11]. However, most previous studies have been limited to pure aluminum or aluminum alloys with restricted compositions, which constrains their applicability to the diverse aluminum alloys widely used in industrial applications [12,13].

In practical industrial applications, not only pure aluminum from the Al 1000 series but also aluminum alloys from the Al 3000, 5000, and 6000 series containing alloying elements such as manganese (Mn), magnesium (Mg), and silicon (Si) are widely used [14-17]. These alloying elements can influence the chemical composition of the oxide film, ion transport characteristics, and oxide dissolution behavior during the anodizing process, thereby significantly affecting the growth rate and structural stability of AAO [18,19]. Nevertheless, systematic comparative studies on AAO formation behavior as a function of alloy composition under identical anodizing conditions remain relatively limited.

In addition, the pore-widening (PW) process performed after anodizing is a key step for controlling the pore diameter and surface porosity of AAO, thereby tuning its wettability and functional properties [20-22]. Previous

†Corresponding author: cjeong@deu.ac.kr
††These authors contributed equally to this work as the first author.
Jisoo Kim: Ph.D. Student, Chanyoung Jeong: Professor

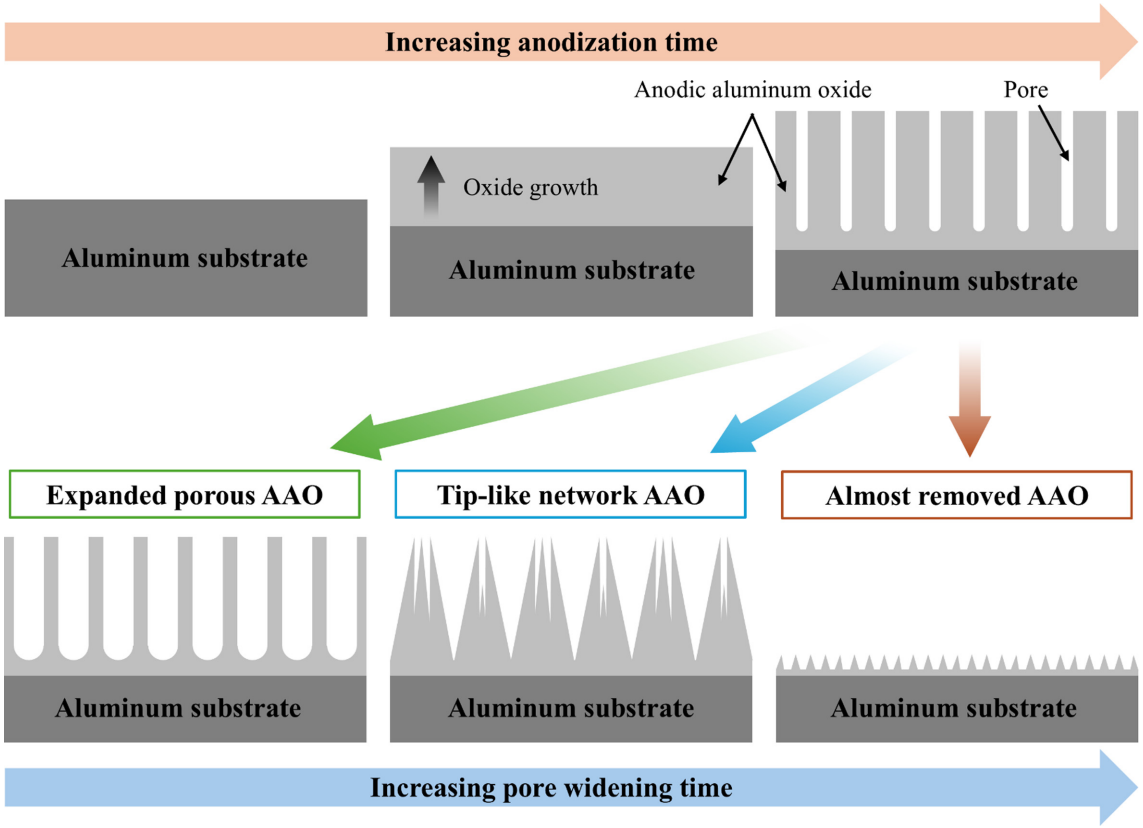

Fig. 1. Schematic illustration of anodic aluminum oxide (AAO) formation and its alloy-dependent structural evolution during pore-widening (PW)

studies have reported that PW leads to an increase in pore diameter and an improvement in wettability [23-25]. However, the oxide film collapse and structural changes that can occur during prolonged PW have not been sufficiently discussed. In particular, although differences in alloy composition can alter the chemical stability of the oxide film and result in distinct PW rates and collapse behaviors [26], these two characteristics have rarely been clearly distinguished and systematically analyzed.

The PW rate represents an indicator describing the rate at which the pore diameter increases with time, whereas the structural stability of the oxide film refers to how long the oxide film can maintain its structure in an acidic solution environment [27-29]. Therefore, even when PW proceeds rapidly, early structural collapse may occur if the chemical stability of the oxide film is low [30]. Conversely, even when PW occurs relatively slowly, a uniform oxide film structure can remain stable for an extended period. From this perspective, it is necessary to separately understand the AAO growth rate, PW rate, and structural collapse behavior.

Accordingly, in this study, AAO films were formed by anodizing Al 1050, Al 3003, Al 5052, and Al 6061 aluminum alloys for 1 h under identical conditions, and the pore structure, oxide-film thickness, and average AAO growth rate were comparatively analyzed as a function of alloy composition. Subsequently, the PW time was varied to observe structural evolution and collapse behavior of AAO, and to clarify the relationship between PW rate and oxide-film structural stability. Furthermore, the correlation between surface porosity or void fraction and water contact angle was analyzed to indirectly evaluate the influence of surface structural changes and wettability on electrolyte penetration behavior. Based on these results, this study aims to elucidate the effect of alloy composition on the wettability behavior of AAO and to provide fundamental guidelines for oxide-film structural design aimed at improving corrosion resistance in future applications.

2. Experimental Methods

2.1 Materials and specimen preparation

In this study, Al 1050, Al 3003, Al 5052, and Al 6061 aluminum alloys were used to compare oxide-film growth behavior and pore-widening (PW) characteristics as a function of alloy composition. The aluminum specimens were plates with a thickness of 1 mm, and the exposed working electrode area for electrochemical reactions was fixed at 7.5 cm^2. To remove surface contaminants, the aluminum specimens were ultrasonically cleaned sequentially in acetone, ethanol, and distilled water for 10 minutes each, followed by drying.

Prior to anodization, electropolishing was performed to remove the native oxide layer and to achieve surface planarization. Electropolishing was carried out for 1 minute at an applied voltage of 20 V in an electrolyte composed of perchloric acid (70%) and ethanol (99%) mixed at a volume ratio of 1:4. Subsequently, anodization was conducted for 1 h at 40 V in a 0.3 M oxalic acid electrolyte maintained at 0 °C, using a platinum plate as the counter electrode. The aluminum specimen and platinum electrode were fixed as the anode and cathode, respectively, and a double-jacketed beaker combined with a cooling chiller was used to maintain the electrolyte temperature.

After anodization, PW was performed by immersing the aluminum specimens in a 0.1 M phosphoric acid solution at 30 °C for 10, 30, and 50 minutes. During the PW process, the phosphoric acid electrolyte was placed on a hot plate to maintain a constant temperature.

2.2 Characterization

The surface morphology of the oxide films formed after anodization and PW was examined using a field emission scanning electron microscope (FE-SEM, IT800, JEOL, Inc., Converging Materials Core Facility, Dong-Eui University). Prior to observation, the specimens were coated with platinum, and FE-SEM imaging was performed at an accelerating voltage of 15 kV. In addition, the surface chemical composition of the oxide films was qualitatively and quantitatively analyzed using an energy dispersive X-ray spectrometer (EDS) attached to the FE-SEM.

The pore diameter (D_p), interpore distance (D_{int}), and oxide-film thickness of anodic aluminum oxide (AAO) were measured from the FE-SEM images using ImageJ software, and the surface porosity was evaluated using the thresholding function. The solid fraction (f_{SL}) is calculated using equation (1), where "a" is the interpore distance and "r" is the pore radius.

$$f_{SL} = 1 - \frac{2\pi r^2}{\sqrt{3}a^2} \quad (1)$$

The average growth rate of AAO formed after 1 h of anodization and the PW rate as a function of PW time were calculated using equation (1) and equation (2), respectively. Here, $D_p(0)$ represents the average pore diameter before PW, and $D_p(t)$ denotes the average pore diameter after a PW time t. To ensure a consistent comparison among alloys, the PW rate was defined as the slope of pore diameter increase within the initial stable widening region (0-10 min), where structural collapse had not yet occurred for all samples.

$$\text{Average AAO growth rate} = \frac{AAO\ thickness}{Anodizing\ time} \quad (2)$$

$$PW\ rate = \frac{D_p(t) - D_p(0)}{t} \quad (3)$$

In this study, "porosity" refers to the area fraction of well-defined pores before structural collapse. After pore merging or collapse, where individual pore boundaries become indistinct, the term "void fraction" is used to represent the total void area including irregular merged regions. In addition, structural stability was discussed in terms of the PW time at which the pore diameter became unmeasurable due to pore merging or structural collapse.

Surface wettability was evaluated using a contact angle meter (SmartDrop, Femtobiomed, Inc.). A 3 μL droplet of distilled water was gently deposited onto the surface of each specimen, and the static water contact angle was measured. The static contact angle was measured 3 s after droplet deposition to minimize time-dependent spreading effects on porous AAO surfaces. For each specimen, the contact angle measurement was repeated five times, and the average value and standard deviation were calculated.

3. Results and Discussion

3.1 AAO formation behavior after 1 h anodization

Fig. 2 and Table 1 present the surface morphology and

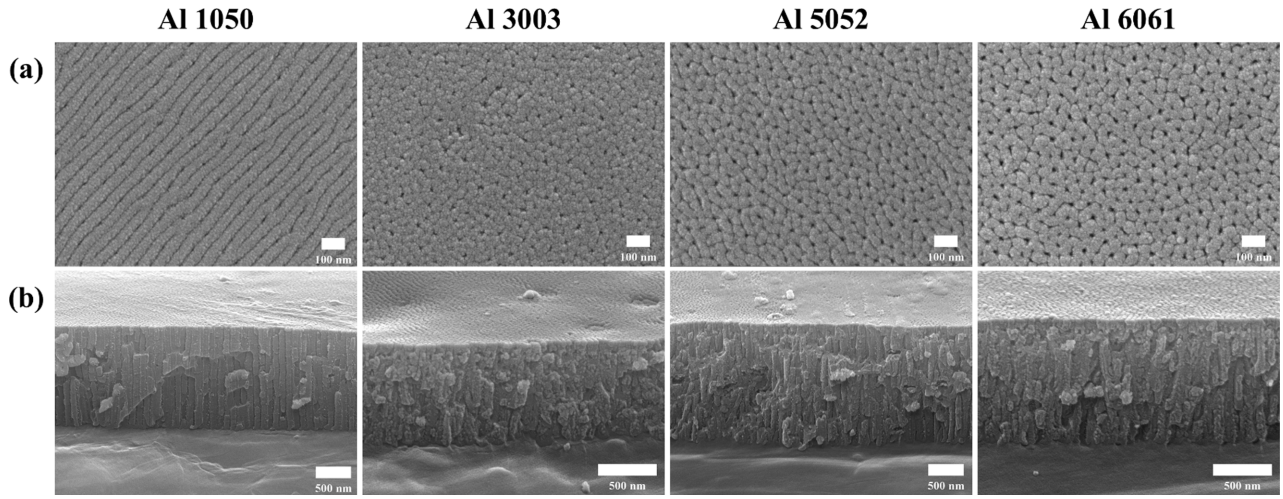

Fig. 2. (a) Top-view and (b) cross-sectional FE-SEM images of anodic aluminum oxide (AAO) films formed on Al 1050, Al 3003, Al 5052, and Al 6061 anodized in 0.3 M oxalic acid at 40 V for 1 h

Table 1. Structural parameters of anodic aluminum oxide (AAO) films formed on Al 1050, Al 3003, Al 5052, and Al 6061 after anodization in 0.3 M oxalic acid at 40 V for 1 h; f_{SL} represents the solid fraction, and the average AAO growth rate was calculated by dividing the final AAO thickness by the anodizing time (1 hour)

Structural parameters	Al 1050	Al 3003	Al 5052	Al 6061
D_p (nm)	7.29 ± 1.32	8.10 ± 1.44	9.70 ± 1.89	11.53 ± 1.32
D_{int} (nm)	68.31 ± 19.80	62.68 ± 15.63	58.79 ± 6.97	56.11 ± 7.39
f_{SL} (%)	99.0	98.5	97.5	96.2
AAO thickness (nm)	1455.13 ± 18.92	844.40 ± 18.63	1719.67 ± 35.04	1053.38 ± 13.02
AAO growth rate (nm/min.)	24.25	14.07	28.66	17.56

Table 2. Surface elemental composition (wt%) of AAO films formed on Al 1050, Al 3003, Al 5052, and Al 6061, determined by EDS analysis after anodization

Element (wt%)	Al 1050	Al 3003	Al 5052	Al 6061
Al	58.35	62.99	55.39	61.25
O	41.65	36.59	43.78	38.07
Mn	-	0.42	-	-
Mg	-	-	0.83	0.21
Si	-	-	-	0.47

quantitative structural characteristics of oxide films formed on Al 1050, Al 3003, Al 5052, and Al 6061 anodized under identical conditions. Typical porous AAO structures were formed on all specimens; however, distinct differences in pore morphology and oxide-film growth behavior were observed depending on the alloy composition. From the top view images in Fig. 2a, Al 1050 exhibited the smallest average pore diameter of 7.29 nm and a relatively uniform pore arrangement. In contrast, the average pore diameter gradually increased for Al 3003, Al 5052, and Al 6061. Correspondingly, the interpore distance (D_{int}) and solid fraction (f_{SL}) showed a decreasing trend, with Al 6061 exhibiting the lowest f_{SL} value. These differences are attributed to changes in the electrochemical characteristics of the barrier layer and oxide dissolution behavior caused by the presence of alloying elements, which alter pore initiation and growth conditions during anodization [31,32].

The cross sectional SEM images in Fig. 2b and the structural parameters listed in Table 1 further reveal that

the oxide-film thickness and growth rate strongly depend on the alloy composition. Al 5052 exhibited the thickest oxide film of 1719.67 nm and the highest average AAO growth rate of 28.66 nm/min, whereas Al 3003 showed the thinnest oxide film of 844.4 nm and the lowest growth rate of 14.07 nm/min. Al 1050 and Al 6061 displayed intermediate growth behavior. These results indicate that alloying elements modify the balance between oxide formation and dissolution reactions, thereby directly influencing the efficiency of oxide-film growth [33,34].

The EDS results summarized in Table 2 provide further insight into these structural differences from a compositional perspective. Al 5052 contains Mg at 0.83 wt%, while Al 6061 contains both Mg at 0.21 wt% and Si at 0.47 wt%. These alloying elements are expected to form Mg-, Si-, and Mn-containing oxides (e.g., MgO and SiO_2) during anodization or produce mixed oxides with Al_2O_3 [35]. The presence of these oxides may alter ion transport properties and the chemical stability of the barrier layer. It should be noted that EDS analysis provides elemental information but cannot directly confirm the chemical states of the oxides; therefore, the presence of Mg-, Si-, and Mn-containing oxides is inferred based on alloy composition and previous literature. In particular, the highest oxide-film growth rate observed for Al 5052 can be attributed to the presence of Mg based oxides, which may exhibit higher ionic conductivity than Al_2O_3 or promote localized dissolution, thus accelerating oxide growth and pore development. In contrast, Al 3003, which contains Mn, exhibited a relatively low oxide growth rate, suggesting that Mn may hinder charge transport in the barrier layer or induce nonuniform oxidation behavior.

3.2 Structural evolution of AAO during pore-widening

Figs. 3-6 show FE-SEM images illustrating the surface morphology and pore structure evolution of AAO formed on Al 1050, Al 3003, Al 5052, and Al 6061 after anodization for 1 h under identical conditions, followed by pore-widening (PW) in a 0.1 M phosphoric acid solution for 0, 10, 30, and 50 minutes. For all alloys, the pore diameter and surface porosity increased with increasing PW time, which is consistent with the quantitative results of D_p, D_{int}, and porosity summarized in Table 3. However, during prolonged PW, the chemical stability of the oxide film varied significantly depending on the alloy composition.

For Al 1050 shown in Fig. 3, the pore diameter increased from 7.29 nm to 51.27 nm as the PW time increased from 0 to 30 minutes. After 50 minutes of PW, the pore walls were dissolved to such an extent that quantitative measurement of the pore diameter and interpore distance was no longer possible, resulting in the formation of an interconnected tip like network structure. Consequently, a well defined porous structure in which D_p and D_{int} could be quantitatively determined was no longer maintained.

Under these conditions, the measured area fraction is more appropriately interpreted as a void fraction,

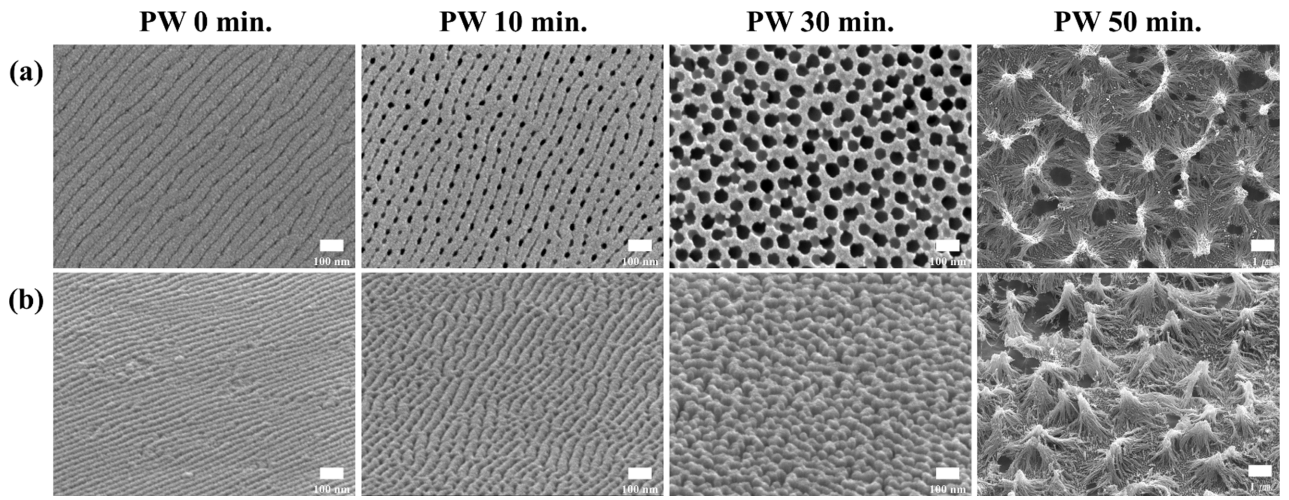

Fig. 3. (a) Top-view and (b) tilted-view FE-SEM images of AAO formed on Al 1050 after pore-widening (PW) for 0, 10, 30, and 50 minutes in 0.1 M phosphoric acid at 30 ºC

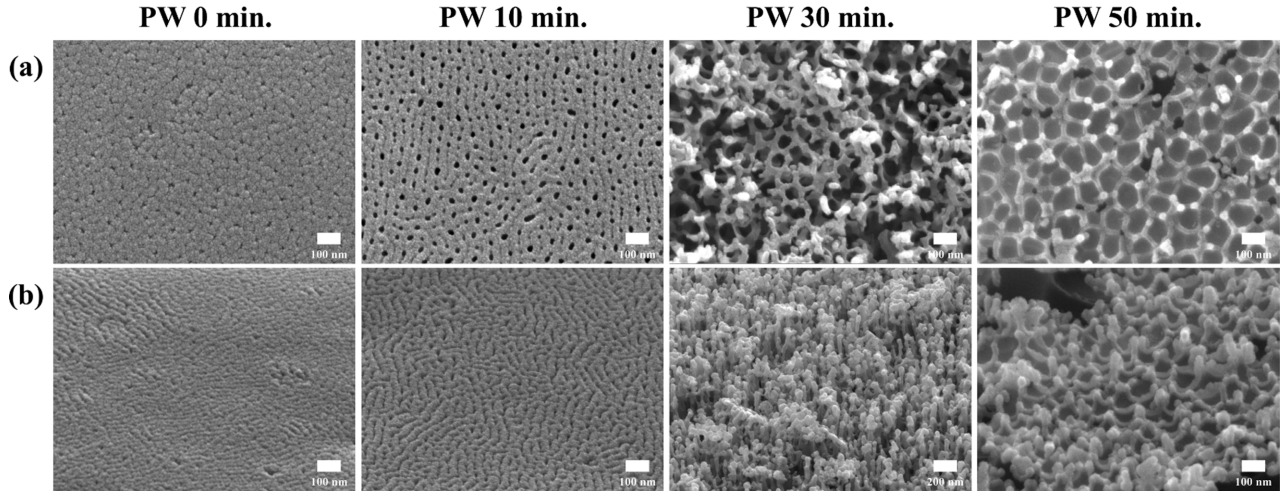

Fig. 4. (a) Top-view and (b) tilted-view FE-SEM images of AAO formed on Al 3003 after pore-widening (PW) for 0, 10, 30, and 50 minutes in 0.1 M phosphoric acid at 30 °C

representing the proportion of empty regions within the collapsed oxide film, rather than porosity based on cylindrical pores. The void fraction was determined to be 82.39%. This behavior indicates that AAO formed on Al 1050 exhibits relatively high chemical stability in acidic solutions. Even as PW progresses, the oxide film does not undergo immediate complete dissolution; instead, pore walls first collapse and reorganize into a tip like network structure, followed by further dissolution at longer PW times. When pore merging or collapse occurs, individual pore boundaries become ill-defined, making D_p and D_{int} measurements increasingly uncertain. Therefore, the observed structural collapse at longer PW times was primarily evaluated based on morphological changes observed in FE-SEM images.

For Al 3003 shown in Fig. 4, the pore diameter increased from 8.10 nm to 16.42 nm up to a PW time of 10 minutes, indicating a typical PW behavior. However, from 30 minutes of PW, rapid dissolution of the pore walls occurred, leading to collapse of the pore structure. Although a porous morphology was still observed, the original cylindrical pore arrangement was no longer preserved, making it impossible to quantitatively define the pore diameter (D_p) and interpore distance (D_{int}). After 50 minutes of PW, the oxide film was almost completely removed, exposing the aluminum substrate, and the surface effectively transitioned to a nonporous state.

Notably, although the PW rate of Al 3003 (0.83 nm/min) was lower than that of Al 1050 (1.13 nm/min), the pore structure of Al 3003 collapsed at an earlier PW time of 30 minutes. This behavior is attributed to the presence of Mn based oxides in the AAO formed on Al 3003, which exhibit relatively low chemical stability in acidic phosphoric acid solutions. As a result, localized dissolution readily occurs within the oxide film, causing premature collapse of the pore walls before sufficient PW can take place.

For Al 5052 shown in Fig. 5, the pore diameter increased rapidly from 9.70 nm to 28.84 nm within 10 minutes of PW, exhibiting the highest PW rate of 1.91 nm/min among the investigated alloys. This rapid PW behavior is attributed to the relatively high solubility of the oxide film formed on Mg containing Al 5052 in phosphoric acid solution, which promotes accelerated dissolution of the pore walls. However, after 30 minutes of PW, both the oxide film and pore structure were almost completely collapsed, making quantitative analysis of the pore structure no longer possible. This behavior may be explained by the possibility that Mg-containing oxides (e.g., MgO or $MgAl_2O_4$), which are expected to be present based on alloy composition and previous reports, are more susceptible to dissolution in acidic environments than Al_2O_3, thereby potentially accelerating PW while simultaneously reducing the structural stability of the oxide film [36,37].

For Al 6061 shown in Fig. 6, a typical PW behavior was observed up to 10 minutes, with the pore diameter increasing from 11.52 nm to 24.04 nm, corresponding to

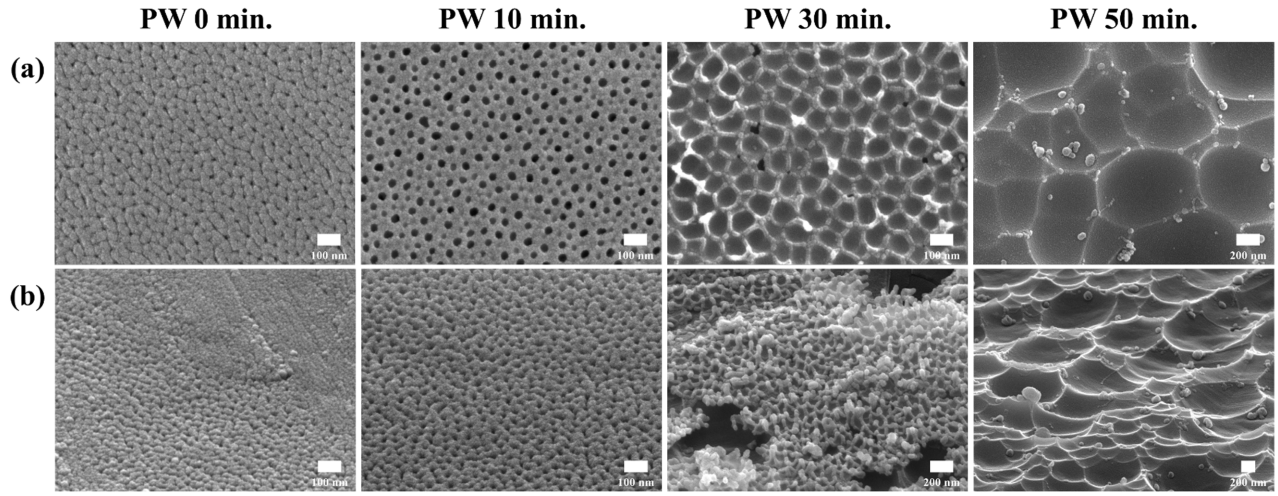

Fig. 5. (a) Top-view and (b) tilted-view FE-SEM images of AAO formed on Al 5052 after pore-widening (PW) for 0, 10, 30, and 50 minutes in 0.1 M phosphoric acid at 30 °C

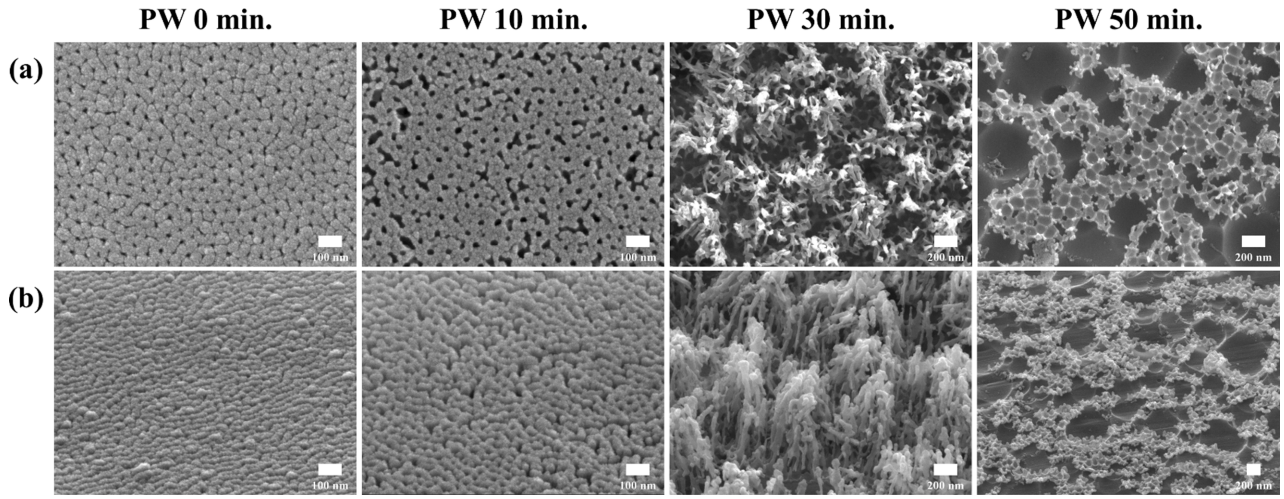

Fig. 6. (a) Top-view and (b) tilted-view FE-SEM images of AAO formed on Al 6061 after pore-widening (PW) for 0, 10, 30, and 50 minutes in 0.1 M phosphoric acid at 30 °C

a PW rate of 1.25 nm/min. For the 30 minutes pore widened Al 6061 specimen, a tip like network structure similar to that observed for Al 1050 after 50 minutes of PW was formed. Under this condition, the measured area fraction is more appropriately interpreted as a void fraction, representing the proportion of empty regions within the collapsed oxide film rather than porosity based on cylindrical pores, and this value was determined to be 61.58%.

After 50 minutes of PW, the oxide film was almost completely removed, and the surface transitioned to a nonporous state. This behavior can be attributed to the chemically heterogeneous oxide film formed on Al 6061 containing both Mg- and Si-related phases, which promotes localized dissolution and micro-galvanic effects in acidic solutions [38].

The EDS results summarized in Table 4 support the observed pore structure collapse behavior. With increasing PW time, all alloys exhibited a pronounced decrease in oxygen content accompanied by an increase in aluminum content, indicating progressive dissolution of the oxide film and exposure of the aluminum substrate. In particular, the specimens of Al 3003 after 50 minutes of PW, Al 5052 after 30 and 50 minutes, and Al 6061 after 50

Table 3. Pore diameter (D_p), interpore distance (D_{int}), porosity, AAO morphology, and initial pore-widening (PW) rate of AAO formed on Al 1050, Al 3003, Al 5052, and Al 6061 after PW for different times (0, 10, 30, and 50 minutes);

Alloy	PW time (min.)	D_p (nm)	D_{int} (nm)	Porosity (%)	AAO morphology	Initial PW rate (nm/min.)
1050	0	7.29 ± 1.33	68.30 ± 19.80	0.69	Porous	1.13
	10	18.59 ± 2.45	62.80 ± 8.49	10.76	Porous	
	30	51.27 ± 3.84	81.94 ± 12.50	43.83	Porous	
	50	N/A	N/A	82.39*	Tip-like network	
3003	0	8.10 ± 1.44	62.68 ± 15.63	1.41	Porous	0.83
	10	16.42 ± 2.29	57.38 ± 15.97	8.85	Porous	
	30	N/A	N/A	48.97*	Locally dissolved	
	50	N/A	N/A	0	Almost removed	
5052	0	9.70 ± 1.89	58.79 ± 6.97	3.01	Porous	1.91
	10	28.84 ± 3.07	65.03 ± 10.64	21.02	Porous	
	30	N/A	N/A	0	Almost removed	
	50	N/A	N/A	0	Removed	
6061	0	11.52 ± 1.32	56.11 ± 7.39	4.75	Porous	1.25
	10	24.04 ± 4.43	56.15 ± 10.11	17.70	Porous	
	30	N/A	N/A	61.58*	Tip-like network	
	50	N/A	N/A	0	Almost removed	

* Void fraction of collapsed or locally dissolved oxide films

Table 4. Surface elemental composition (wt%) of AAO formed on Al 1050, Al 3003, Al 5052, and Al 6061 after pore-widening (PW), determined by EDS analysis

Alloy	PW time (min.)	Al	O	Mn	Mg	Si
1050	0	58.35	41.65	-	-	-
	10	59.35	40.65	-	-	-
	30	65.65	34.35	-	-	-
	50	94.77	5.23	-	-	-
3003	0	62.99	36.59	0.42	-	-
	10	65.34	33.94	0.71	-	-
	30	85.30	13.48	1.22	-	-
	50	96.35	3.07	0.58	-	-
5052	0	55.39	43.78	-	0.83	-
	10	60.22	38.71	-	1.07	-
	30	94.85	2.75	-	2.39	-
	50	96.11	1.45	-	2.43	-
6061	0	61.25	38.07	-	0.21	0.47
	10	68.64	30.57	-	0.32	0.47
	30	89.94	8.82	-	0.66	0.59
	50	97.11	1.69	-	0.69	0.51

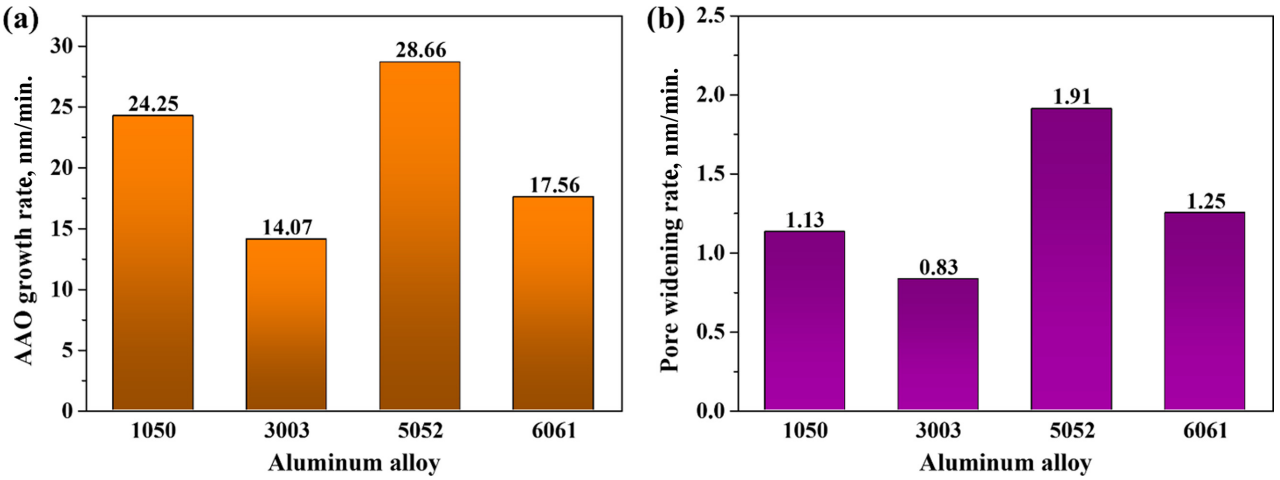

Fig. 7. (a) Average AAO growth rate and (b) pore-widening (PW) rate of AAO formed on Al 1050, Al 3003, Al 5052, and Al 6061

minutes showed oxygen contents reduced to approximately 1-3 wt%, confirming that the AAO layer was almost completely removed under these conditions.

In contrast, Al 1050 retained a relatively high oxygen content even after 50 minutes of PW, demonstrating a higher degree of residual oxide film. This result suggests that AAO formed on pure aluminum exhibits the highest chemical stability among the investigated alloys in acidic phosphoric acid solution.

Fig. 7 compares the average AAO growth rate during anodization and the PW rate of AAO in phosphoric acid for Al 1050, Al 3003, Al 5052, and Al 6061, and both parameters exhibit clear differences depending on the alloy composition.

The AAO growth rate shown in Fig. 7a was the highest for Al 5052 at 28.66 nm/min and the lowest for Al 3003 at 14.07 nm/min. This behavior can be attributed to the oxide film formed on Mg containing Al 5052, which exhibits high ionic conductivity and enhanced oxidation reactivity, leading to rapid oxide-film formation. In contrast, the oxidation reaction of Al 3003, which contains Mn, is relatively suppressed. Al 1050 and Al 6061 exhibited intermediate growth behavior between these two extremes.

The PW rate shown in Fig. 7b was also the highest for Al 5052 at 1.91 nm/min and the lowest for Al 3003 at 0.83 nm/min. This trend can be explained by the fact that Mg based oxides dissolve more readily than Al_2O_3 in phosphoric acid, thereby accelerating PW, whereas the oxide film formed on Al 3003 containing Mn undergoes PW more slowly.

However, comparison with the pore structure collapse behavior discussed above reveals that the PW rate and the structural stability of the oxide film are independent characteristics. Although Al 3003 exhibited the lowest PW rate, premature structural collapse occurred at a PW time of 30 minutes, which is attributed to the low chemical stability of the mixed oxide film containing Mn based oxides, leading to facile localized dissolution. In contrast, Al 1050, despite exhibiting a relatively high PW rate, showed a gradual collapse mechanism involving the formation of a tip like network structure due to its uniform Al_2O_3 based oxide film. As a result, the AAO structure was maintained for a prolonged PW duration.

Therefore, Fig. 7 collectively demonstrates that the AAO growth rate and PW rate in aluminum alloys are governed by the chemical composition of the oxide film, whereas the actual onset and mode of structural collapse are determined by the chemical stability of the oxide film. This finding indicates that alloy composition is a key factor not only in controlling the microstructure of AAO but also in determining its structural stability during prolonged PW processes.

3.3 Wettability evolution and its correlation with surface structure

Fig. 8 show the variation in water contact angle as a function of PW time for Al 1050, Al 3003, Al 5052, and Al 6061, while Fig. 9 summarize the correlation between surface porosity (or void fraction) and contact

angle for the same specimens. For all alloys, the contact angle initially decreased with increasing PW time, indicating enhanced wettability. However, upon prolonged PW, a common trend of wettability reversal was observed due to collapse of the oxide film.

For Al 1050 shown in Fig. 8a and Fig. 9a, the water contact angle continuously decreased from 25.11° to 14.93° as the PW time increased from 0 to 30 minutes. This behavior is attributed to the increase in surface porosity from 0.69% to 43.83% resulting from pore expansion and corresponds to a typical Wenzel wetting behavior, in which increased surface roughness enhances wettability [39,40]. After 50 minutes of PW, collapse of the pore walls led to the formation of a tip-like network structure, allowing the water droplet to infiltrate into the surface and resulting in near-zero contact angles indicative of superhydrophilic behavior. In this study, a near-zero contact angle is defined as a measured contact angle below 5°, indicating a superhydrophilic surface. This enhanced wetting is not governed by conventional pore-based porosity but rather by the high void fraction generated by the collapsed network structure, which maximizes liquid infiltration [41].

For Al 3003 shown in Fig. 8b and Fig. 9b, the contact angle decreased from 24.89° to 12.07° up to 30 minutes of PW as the surface porosity increased. However, after 50 minutes of PW, the contact angle sharply increased to 39.80° due to near-complete removal of the oxide film. This behavior arises from exposure of the aluminum substrate caused by localized dissolution of the oxide film, resulting in the dominance of metallic surface characteristics rather than those of a porous oxide surface.

For Al 5052 shown in Fig. 8c and Fig. 9c, the contact

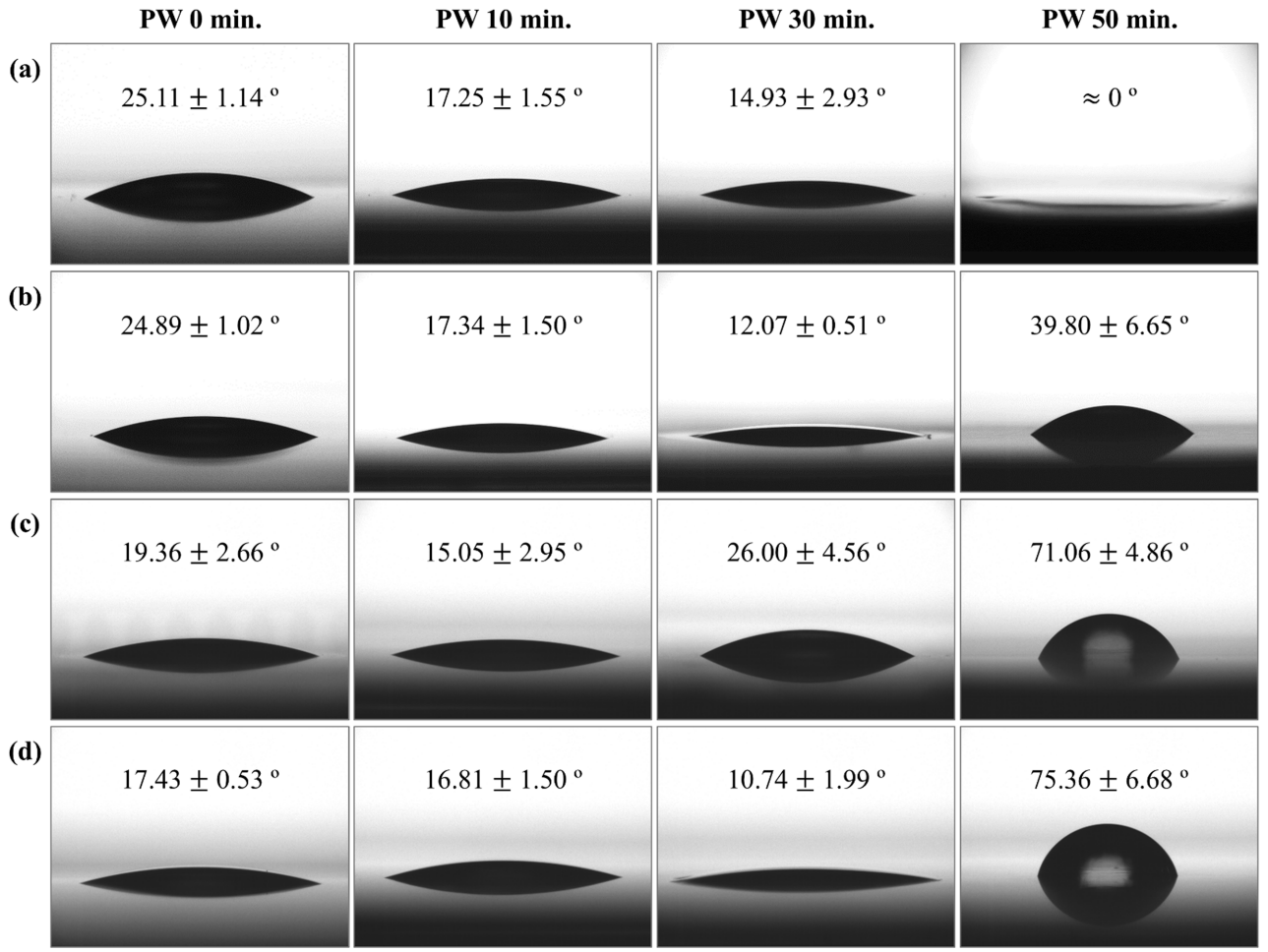

Fig. 8. Water contact angle images of AAO formed on (a) Al 1050, (b) Al 3003, (c) Al 5052, and (d) Al 6061 after pore-widening (PW) for 0, 10, 30, and 50 minutes in 0.1 M phosphoric acid at 30°C

Table 5. Water contact angle values of AAO formed on Al 1050, Al 3003, Al 5052, and Al 6061 after pore-widening (PW) for 0, 10, 30, and 50 min in 0.1 M phosphoric acid at 30 °C

Alloy	PW 0 min.	PW 10 min.	PW 30 min.	PW 50 min.
1050	25.11 ± 1.14°	17.25 ± 1.55°	14.93 ± 2.93°	≈ 0°
3003	24.89 ± 1.02°	17.34 ± 1.50°	12.07 ± 0.51°	39.80 ± 6.65°
5052	19.36 ± 2.66°	15.05 ± 2.95°	26.00 ± 4.56°	71.06 ± 4.86°
6061	17.43 ± 0.53°	16.81 ± 1.50°	10.74 ± 1.99°	75.36 ± 6.68°

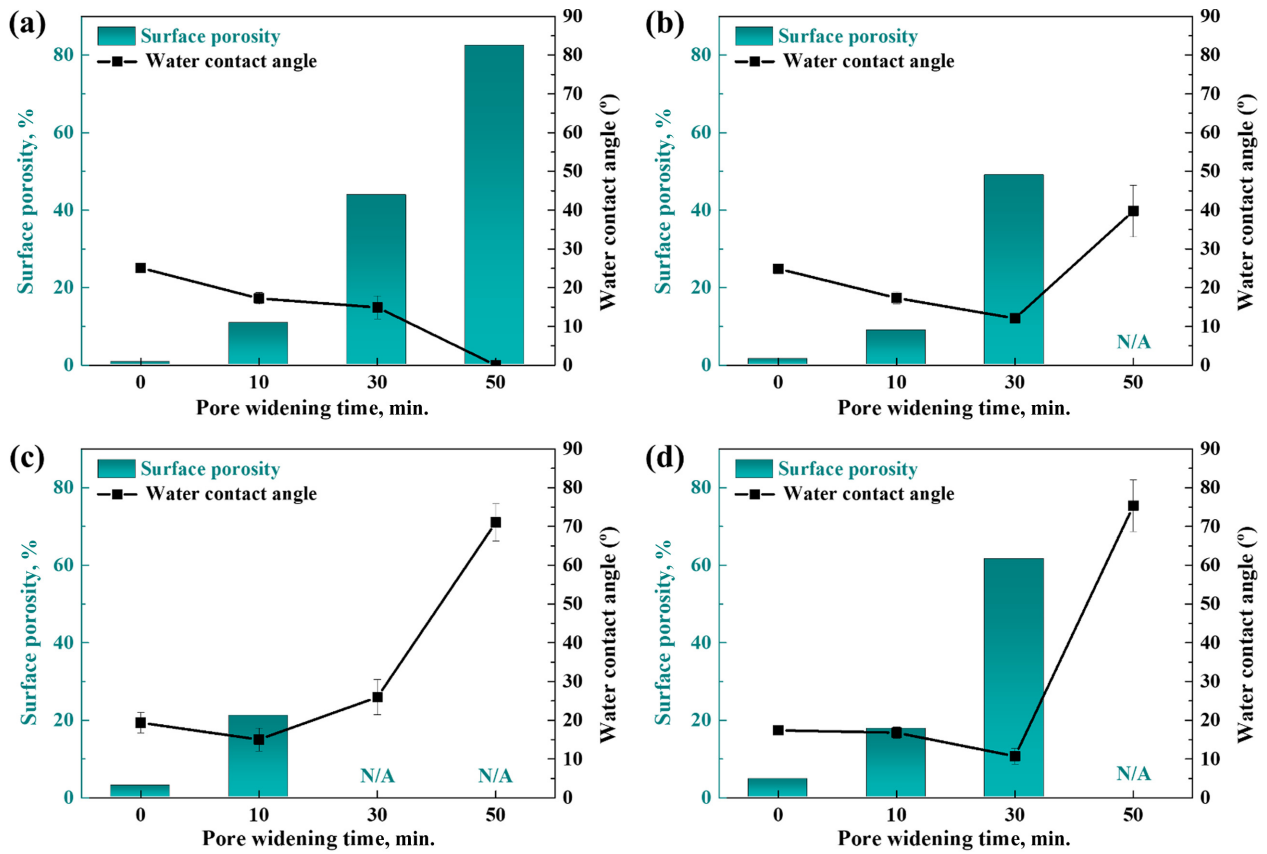

Fig. 9. Correlation between surface porosity (or void fraction) and water contact angle as a function of pore-widening (PW) time for AAO formed on (a) Al 1050, (b) Al 3003, (c) Al 5052, and (d) Al 6061

angle initially decreased up to 10 minutes of PW due to pore expansion. However, after 30 minutes of PW, the contact angle increased sharply to 26.00° and 71.06° as a result of oxide-film collapse and removal. This behavior is attributed to the rapid dissolution of the Mg-containing oxide film in phosphoric acid, which prevents the maintenance of a porous structure and instead leads to a deterioration of wettability.

Similarly, Al 6061 shown in Fig. 8d and Fig. 9d exhibited improved wettability up to 30 minutes of PW, with the contact angle decreasing from 17.43° to 10.74°. In contrast, after 50 minutes of PW, the contact angle increased sharply to 75.36° due to collapse and removal of the oxide film. This behavior can be attributed to the rapid elimination of the chemically heterogeneous mixed oxide film containing Si and Mg through localized dissolution and structural collapse.

Overall, an increase in surface porosity induced by PW led to enhanced wettability for all alloys. However, once the oxide film collapsed or was removed, the wettability behavior reversed and the contact angle increased again. This indicates that wettability is

governed not simply by porosity but by the structural stability of the oxide film and the resulting surface morphology [42]. In particular, the tip-like network structure formed through uniform collapse and rearrangement of pore walls provides continuous capillary pathways and high surface energy simultaneously, thereby maximizing liquid infiltration and acting as the structure that exhibits the most superior wettability. In contrast, when the oxide film is locally removed and the aluminum substrate is exposed, the porous structure is no longer maintained, leading to a deterioration in wettability.

4. Conclusions

In this study, anodic aluminum oxide (AAO) films formed by anodizing Al 1050, Al 3003, Al 5052, and Al 6061 aluminum alloys for 1 h under identical conditions were systematically investigated to compare their structural characteristics and growth behavior. Subsequently, the structural evolution and wettability behavior of AAO were analyzed as a function of pore-widening (PW) time.

Despite the use of identical anodizing conditions, pronounced differences in pore diameter, interpore distance, oxide-film thickness, and average AAO growth rate were observed depending on the alloy composition. In particular, Al 5052, which contains Mg, exhibited the highest AAO growth rate and PW rate, whereas Al 3003, containing Mn, showed relatively low growth rates. These results indicate that alloying elements directly influence oxide-film formation and dissolution reactions, thereby governing the growth behavior of AAO.

During the PW process, all alloys initially exhibited an increase in pore diameter and surface porosity with increasing PW time. However, during prolonged PW, distinct oxide-film collapse behaviors were observed depending on the alloy composition. Al 1050 exhibited a gradual collapse behavior in which the pore walls uniformly collapsed and reorganized into a tip-like network structure, whereas Al 3003 and Al 5052 showed early removal of the oxide film at relatively short PW times due to localized dissolution. Al 6061 exhibited an intermediate collapse behavior between these two types, clearly demonstrating the dependence of oxide-film collapse mechanisms on alloy composition.

The wettability analysis revealed that, within the regime where a well-defined porous AAO structure was maintained, an increase in surface porosity led to a decrease in water contact angle, indicating enhanced wettability. However, once the oxide film collapsed or was removed, the wettability behavior reversed and the contact angle increased again. In particular, specimens forming a tip-like network structure exhibited the most superior wettability due to the formation of continuous capillary pathways, whereas specimens in which the oxide film was removed and the aluminum substrate was exposed showed deteriorated wettability.

This study experimentally demonstrates that the PW rate and the structural stability of the oxide film are governed by different mechanisms, and identifies alloy composition as a key factor determining the growth behavior, collapse characteristics, and wettability of AAO. These findings provide fundamental insights for structural design of AAO formed on aluminum alloys and for optimization of long term PW processes, and are expected to offer important guidelines for the development of functional and superhydrophilic surfaces. Furthermore, the wettability behavior observed in this study is also meaningful in relation to corrosion performance. In particular, the tip-like network structure, which provides continuous microstructural features and high surface roughness simultaneously, is expected to enable the realization of highly water-repellent or superhydrophobic surfaces when combined with post-treatment coatings using low-surface-energy materials. Such structure–coating combinations are anticipated to effectively suppress electrolyte access to the surface, thereby contributing to enhanced long-term corrosion resistance.

References

1. Y. Choi, J. Kim, C. Jeong, Optimization of the Barrier Oxide Layer to Enhance Long-term Corrosion Resistance of SUS 316L Stainless Steel in 3.5 wt% NaCl Solution, *Journal of Materials Science*, **60**, 8148 (2025). Doi: https://doi.org/10.1007/s10853-025-10916-4
2. Y. Choi, C. Jeong, Correlation of oxide film thickness

with interference coloration and corrosion resistance in anodized titanium, *Electrochimica Acta*, **545**, 147737 (2025). Doi: https://doi.org/10.1016/j.electacta.2025.147737
3. A. K. Eessaa, A. M. El-Shamy, Review on fabrication, characterization, and applications of porous anodic aluminum oxide films with tunable pore sizes for emerging technologies, *Microelectronic Engineering*, **279**, 112061 (2023). Doi: https://doi.org/10.1016/j.mee.2023.112061
4. G. E. J. Poinern, N. Ali, D. Fawcett, Progress in nano-engineered anodic aluminum oxide membrane development, *Materials*, **4**, 487 (2011). Doi: https://doi.org/10.3390/ma4030487
5. S. Liu, J. Tian, W. Zhang, Fabrication and application of nanoporous anodic aluminum oxide: A review, *Nanotechnology*, **32**, 222001 (2021). Doi: https://doi.org/10.1088/1361-6528/abe25f
6. W. Lee, S. J. Park, Porous anodic aluminum oxide: anodization and templated synthesis of functional nanostructures, *Chemical reviews*, **114**, 7487 (2014). Doi: https://doi.org/10.1021/cr500002z
7. Y. Choi, C. Jeong, Influence of Electrolyte on the Shape and Characteristics of TiO_2 during Anodic Oxidation of Titanium, *Corrosion Science and Technology*, **22**, 193 (2023). Doi: https://doi.org/10.14773/cst.2023.22.3.193
8. I. Dobosz, Influence of the anodization conditions and chemical treatment on the formation of alumina membranes with defined pore diameters, *Journal of Porous Materials*, **28**, 1011 (2021). Doi: https://doi.org/10.1007/s10934-021-01052-w
9. J. Kim, C. Jeong, Research on variation in nanopore parameters and surface characteristics of anodic aluminum oxide (AAO) films with time-controlled anodization processes, *Journal of Materials Science*, **59**, 10556 (2024). Doi: https://doi.org/10.1007/s10853-024-09806-y
10. C. Jeong, A Study on Functional Hydrophobic Stainless Steel 316L Using Single-Step Anodization and a Self-Assembled Monolayer Coating to Improve Corrosion Resistance, *Coatings*, **12**, 395 (2022). Doi: https://doi.org/10.3390/coatings12030395
11. K. Nielsch, J. Choi, K. Schwirn, R. B. Wehrspohn, U. Gösele, Self-ordering regimes of porous alumina: the 10 porosity rule, *Nano letters*, **2**, 677 (2002). Doi: https://doi.org/10.1021/nl025537k
12. L. Zaraska, G. D. Sulka, J. Szeremeta, M. Jaskuła, Porous anodic alumina formed by anodization of aluminum alloy (AA1050) and high purity aluminum, *Electrochimica Acta*, **55**, 4377 (2010). Doi: https://doi.org/10.1016/j.electacta.2009.12.054
13. E. Razzouk, D. Koncz-Horváth, T. I. Török, Critical Challenges in the Anodizing Process of Aluminium–Silicon Cast Alloys—A Review, *Crystals*, **14**, 617 (2024). Doi: https://doi.org/10.3390/cryst14070617
14. J. Kim, C. Jeong, A Study on the Surface Properties and Corrosion Behavior of Functional Aluminum 3003 Alloy using Anodization Method, *Corrosion Science and Technology*, **21**, 290 (2022). Doi: https://doi.org/10.14773/cst.2022.21.4.290
15. H. Ji and C. Jeong, Fabrication of Superhydrophobic Aluminum Alloy Surface with Hierarchical Pore Nanostructure for Anti-Corrosion, *Corrosion Science and Technology*, **18**, 228 (2019). Doi: https://doi.org/10.14773/cst.2019.18.6.228
16. S. Barua, M. A. Rahman, K. Chandra Bhowmik, I. Khan, Corrosion Resistance of Anodized and Composite-Coated Aluminum Alloys: A Comprehensive Review on 5xxx and 6xxx Series, *Advances in Materials Science and Engineering*, **2025**, 7941108 (2025). Doi: https://doi.org/10.1155/amse/7941108
17. J. Kim, C. Jeong, Investigation of Functional 6061 Aluminum Alloy Oxide Film with Anodization Voltage and Its Corrosion Resistance, *Corrosion Science and Technology*, **22**, 399 (2023). Doi: https://doi.org/10.14773/cst.2023.22.6.399
18. S. A. N. O. Takuma, A. S. O. H. Hidetaka, Effect of alloying elements on the morphology of anodic films formed on 7075 aluminum alloys tempered under different conditions via anodization in sulfuric acid, *Results in Surfaces and Interfaces*, 100650 (2025). Doi: https://doi.org/10.1016/j.rsurfi.2025.100650
19. M. Paz Martínez-Viademonte, S. T. Abrahami, T. Hack, M. Burchardt, H. Terryn, A review on anodizing of aerospace aluminum alloys for corrosion protection, *Coatings*, **10**, 1106 (2020). Doi: https://doi.org/10.3390/coatings10111106
20. Y. Choi, C. Jeong, Investigating the Influence of Pore widening Time Control in Electrochemical Anodization for the Formation of Hybrid Titanium Nanostructures with Enhanced Superhydrophobicity for Improved Corrosion Resistance Efficiency, *Electrochimica Acta*, **492**, 144380 (2024). Doi: https://doi.org/10.1016/j.electacta.2024.144380
21. Y. C. Lin, L. R. Lee, Y. C. Liu, B. Gautam, J. H. Ho, T. H. Tsai, J. T. Chen, Advancing Nanopore Technology: Anodic Aluminum Oxide Membranes with Anisotropic

Pores through Controlled Stretching for Applications in Nanopatterning, *ACS Applied Nano Materials*, **7**, 14707 (2024). Doi: https://doi.org/10.1021/acsanm.4c02257
22. K. M. Chahrour, N. M. Ahmed, M. R. Hashim, N. G. Elfadill, A. M. Al-Diabat, M. Bououdina, Influence of wet etching time cycles on morphology features of thin porous Anodic Aluminum oxide (AAO) template for nanostructure's synthesis, *Journal of Physics and Chemistry of Solids*, **87**, 1 (2015). Doi: https://doi.org/10.1016/j.jpcs.2015.07.020
23. Y. Choi, C. Jeong, Nano-engineering of hybrid titanium oxide structure (TiO2) using pore-widening concentration for enhanced superhydrophilicity, *Corrosion Science and Technology*, **23**, 41 (2024). Doi: https://doi.org/10.14773/cst.2024.23.1.41
24. C. Jeong, J. Jung, K. Sheppard, C. H. Choi, Control of the Nanopore Architecture in Anodic Alumina via Stepwise Anodization with Voltage Modulation and pore widening, *Nanomaterials*, **13**, 342 (2023). Doi: https://doi.org/10.3390/nano13020342
25. C. Jeong, J. Lee, K. Sheppard, C. H. Choi, Air-impregnated Nanoporous Anodic Aluminum Oxide Layers for Enhancing the Corrosion Resistance of Aluminum, *Langmuir*, **31**, 11040 (2015). Doi: https://doi.org/10.1021/acs.langmuir.5b02392
26. C. A. Ku, C. Y. Yu, C. W. Hung, C. K. Chung, Advances in the fabrication of nanoporous anodic aluminum oxide and its applications to sensors: a review, *Nanomaterials*, **13**, 2853 (2023). Doi: https://doi.org/10.3390/nano13212853
27. Y. Choi, C. Jeong, Improving Insulating and Wettability Properties of Titanium Alloys via Electrochemical Anodization, *Corrosion Science and Technology*, **24**, 151 (2025). Doi: https://doi.org/10.14773/cst.2025.24.3.151
28. M. M. Rahman, E. Garcia-Caurel, A. Santos, L. F. Marsal, J. Pallarès, J. Ferré-Borrull, Effect of the anodization voltage on the pore-widening rate of nanoporous anodic alumina, *Nanoscale research letters*, **7**, 474 (2012). Doi: https://doi.org/10.1186/1556-276X-7-474
29. M. Iwai, T. Kikuchi, Chemical stability of porous anodic aluminum oxide in both acidic and alkaline solutions, *Thin Solid Films*, **771**, 139784 (2023). Doi: https://doi.org/10.1016/j.tsf.2023.139784
30. A. Belwalkar, E. Grasing, W. Van Geertruyden, Z. Huang, W. Z. Misiolek, Effect of processing parameters on pore structure and thickness of anodic aluminum oxide (AAO) tubular membranes, *Journal of membrane science*, **319**, 192 (2008). Doi: https://doi.org/10.1016/j.memsci.2008.03.044
31. H. Yanagimoto, K. Saito, H. Takahashi, M. Chiba, Changes in the structure and corrosion protection ability of porous anodic oxide films on pure Al and Al alloys by pore sealing treatment, *Materials*, **15**, 8544 (2022). Doi: https://doi.org/10.3390/ma15238544
32. Y. Park, C. Jeong, Comparison of Hydrophobicity and Corrosion Properties of Aluminum 5052 and 6061 Alloys After Anodized Surface Treatment, *Corrosion Science and Technology*, **21**, 200 (2022). Doi: https://doi.org/10.14773/cst.2022.21.3.200
33. J. Wang, R. Zhao, M. Xu, G. Chen, Cathodic electrochemiluminescence of luminol in aqueous solutions based on C-doped oxide covered titanium electrode, *Electrochimica acta*, **56**, 74 (2010). Doi: https://doi.org/10.1016/j.electacta.2010.09.055
34. F. Zhang, C. Örnek, J. O. Nilsson, J. Pan, Anodisation of aluminium alloy AA7075–Influence of intermetallic particles on anodic oxide growth, *Corrosion Science*, **164**, 108319 (2020). Doi: https://doi.org/10.1016/j.corsci.2019.108319
35. J. M. Torrescano-Alvarez, M. Curioni, H. Habazaki, T. Hashimoto, P. Skeldon, X. Zhou, Incorporation of alloying elements into porous anodic films on aluminium alloys: The role of cell diameter, *Electrochimica Acta*, **296**, 783 (2019). Doi: https://doi.org/10.1016/j.electacta.2018.11.041
36. A. Fedoročková, P. Raschman, Effects of pH and acid anions on the dissolution kinetics of MgO, *Chemical Engineering Journal*, **143**, 265 (2008). Doi: https://doi.org/10.1016/j.cej.2008.04.029
37. M. D. Franke, W. R. Ernst, A. S. Myerson, Kinetics of dissolution of alumina in acidic solution, *AIChE journal*, **33**, 267 (1987). Doi: https://doi.org/10.1002/aic.690330213
38. I. Tsangaraki-Kaplanoglou, S. Theohari, T. Dimogerontakis, Y. M. Wang, H. H. H. Kuo, S. Kia, Effect of alloy types on the anodizing process of aluminum, *Surface and Coatings Technology*, **200**, 2634 (2006). Doi: https://doi.org/10.1016/j.surfcoat.2005.07.065
39. R. N. Wenzel, Resistance of solid surfaces to wetting by water, *Industrial & engineering chemistry*, **28**, 988 (1936). Doi: https://doi.org/10.1021/ie50320a024
40. J. G. Buijnsters, R. Zhong, N. Tsyntsaru, J. P. Celis, Surface wettability of macroporous anodized aluminum oxide, *ACS applied materials & interfaces*, **5**, 3224 (2013). Doi: https://doi.org/10.1021/am4001425
41. D. Quéré, Wetting and roughness, *Annual Review of*

Materials Research, **38**, 71 (2008). Doi: https://doi.org/10.1146/annurev.matsci.38.060407.132434

42. C. Jeong, C. H. Choi, Single-step Direct Fabrication of Pillar-on-pore Hybrid Nanostructures in Anodizing Aluminum for Superior Superhydrophobic Efficiency, *ACS Applied Materials & Interfaces*, **4**, 842 (2012). Doi: https://doi.org/10.1021/am201514n